Marine Structures 93 (2024) 103542

Contents lists available at ScienceDirect

Marine Structures

journal homepage: www.elsevier.com/locate/marstruc

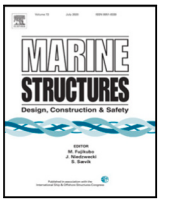

Moored elastic sheets under the action of nonlinear waves and current

Vasily K. Kostikov [a], Masoud Hayatdavoodi [a,b,*], R. Cengiz Ertekin [a,c]

[a] College of Shipbuilding Engineering, Harbin Engineering University, Harbin, China
[b] School of Science and Engineering, University of Dundee, Dundee DD1 4HN, UK
[c] Ocean and Resources Engineering Department, University of Hawaii, Honolulu, Hawaii 96822, USA

ARTICLE INFO

Keywords:
Floating solar panels
Floating airports
Mooring lines
Green–Naghdi equations
Elastic sheet
Wave–structure interaction

ABSTRACT

This study is concerned with the interaction between nonlinear water waves and uniform current with moored, floating elastic sheets, resembling floating solar panels, floating airports, tunnels and bridges, and floating energy systems. The Green–Naghdi theory is applied for the nonlinear wave–current motion, the thin plate theory is used to determine the deformations of the elastic sheet and Hooke's law defines the effect of the mooring lines. The horizontal displacement of the floating sheet is determined by substituting the forces induced by the fluid flow and the tensions generated in the mooring lines into the equations of motion of the floating body. The resulting governing equations, boundary and matching conditions are solved in two dimensions with a finite-difference technique. The results are compared with the available numerical data. Overall, very good agreement is observed. In the model developed here, the sheet is allowed to drift due to the wave–current impact, and hence the mooring lines partially restrict both deformation and the horizontal motions of the sheet. The influence of the mooring lines on the dynamics of the floating sheet is assessed in terms of wave- and current-induced elastic deformations and surge movements of the sheet. It is demonstrated that the mooring lines attached to the leading and trailing edges of the sheet can be highly effective in mitigating the horizontal oscillations and vertical elastic deformations of the floating sheet subjected to the wave and current actions. Special attention is given to the horizontal periodic motions of the sheet, which are analysed by use of a Fourier transform technique. It is shown that the moored elastic sheet can oscillate at a frequency different from its exciting frequency as a result of restoring forces from the mooring lines, exciting resonance when both frequencies meet. Extensive study in a broad range of sheet parameters, mooring stiffnesses and wave–current conditions established the location of resonant regimes of different configurations of the moored systems. Analysis of wave reflection and transmission coefficient revealed that mooring lines of increasing stiffness intensify the wave reflection and, consequently, result in smaller energy transformation downwave.

1. Introduction

In recent decades, the research on very large floating structures (VLFS), having large horizontal dimensions compared to the thickness, and hence exhibiting elastic behaviour, has received considerable amount of attention. Hydroelastic effects can be important in the design of floating offshore wind turbines, floating airports, pipelines, bridges, and even space-vehicles launch

* Corresponding author at: School of Science and Engineering, University of Dundee, Dundee DD1 4HN, UK.
E-mail address: mhayatdavoodi@dundee.ac.uk (M. Hayatdavoodi).

https://doi.org/10.1016/j.marstruc.2023.103542
Received 8 September 2022; Received in revised form 1 October 2023; Accepted 7 November 2023

sites, because the elastic deformations can alter the loads on the structure and its operational limits. The growing trend in the renewable energy sector is floating power plants, consisting of solar panels installed on the buoyant basement [1]. This concept address the challenges raised by the land scarcity in the areas with high population density and increasing demands for renewable energy. For this new technology, it is essential to design the mooring and anchoring systems which will help to withstand strong waves, current and wind effects [2]. Mooring systems can also be effective in mitigation of the structural response of a deformable structure. Understanding the forces acting on the mooring lines and accurate prediction of the wave- and current-induced motions of a moored deformable body are important subjects to coastal and ocean engineers. To assess the magnitude of motions of the moored structure and loads in the mooring system, an appropriate model capable of capturing the loads and responses is essential, and this is the aim of the present study.

To clarify the principal differences between the existing theoretical models and highlight the contribution of the present paper, we introduce here the following four different combinations of a floating sheet with or without mooring lines, fixed or free to move in the horizontal direction.

Unmoored fixed sheet. There has been a significant progress in the literature on the topic of wave interaction with unmoored floating elastic structures, where the main interest is confined to the wave-induced elastic deformations of the structure and transformation of the ambient wave field, see [3–9]. The above mentioned works studied the hydroelastic response of the floating elastic sheets under the common assumption that the sheet is somehow fixed so that it cannot move horizontally, but can bend without any restraints.

Unmoored free sheet. The subject of a floating elastic sheet which is allowed to drift in the horizontal direction freely, in the absence of any restraints and mooring lines, still remains mostly unexplored. The existing studies focus on the dynamics of a rigid box and use the slope-sliding model [10,11], requiring large wavelength to plate length ratio, or rather time-consuming smoothed-particle hydrodynamics method [12]. We have proposed an effective model of the free drift of a floating elastic sheet by the action of waves and current and further developed it to the case of multiple sheets, see [13,14]. The detailed review of the methods and solutions to the problem of the free drift of floating structures can also be found there.

Moored fixed sheet. The problem of wave interaction with moored deformable structures is commonly investigated by assuming that these structures cannot be displaced horizontally. The main interest of such studies is confined to the effect of mooring lines on structural elastic deformations of the floating body. Khabakhpasheva and Korobkin [15] used the eigenfunction technique with the basic functions replaced by trigonometric functions and found that spring connection of the floating beam to the sea bottom can sufficiently reduce the deflections of the plate, if the rigidity of the spring is properly selected. Karmakar and Soares [16] used the ordinary eigenfunction expansion method to investigate the problem of wave scattering by a floating plate connected by mooring lines in shallow and finite water depths. Karperaki et al. [17] introduced multiple spring-dashpot connectors installed at different points along the structure. They illustrated that response mitigation can be achieved by increasing the number and stiffness of the employed connectors. Nguyen et al. [18] sought for the optimal mooring stiffnesses with a complex optimization algorithm and found that the effectiveness of the mooring lines decreases from a certain critical value of wavelength. Mohapatra and Soares [19] added mooring-edge boundary conditions to a more efficient boundary-integral equation method utilizing Green's theorem, alternative to boundary-element (BEM) and finite-element (FEM) methods commonly applied to the hydroelasticity problems. These research studies were based on the potential-flow theory, and the solutions were obtained in the frequency domain from the linearized equations. In this paper, we follow these approaches only in terms of the boundary conditions, where the transverse component of the tension at the plate edges is confined to the restoring force of the mooring line, and investigate the effect of nonlinear waves and current on such structures.

Moored free sheet. The subject of study concerned with the motion response of a moored deformable structure in both horizontal and vertical directions due to the stretching of the mooring lines has not yet been fully developed. The lack of theoretical models in this field is particularly due to the difficulties of the hydroelasticity problem where the coupled hydrodynamics and structural dynamics problems need to be solved simultaneously. In contrast, the dynamics of a moored rigid body below or above the free surface has been extensively investigated by many researchers. Sannasiraj et al. [20] adopted two-dimensional finite-element model to investigate the dynamics of a pontoon-type floating breakwater in three modes of motion: sway, heave and roll. Rahman et al. [21] described the dynamics of a moored breakwater under the wave action, by use of a numerical model based on Navier–Stokes equations, that combines the volume of fluid method and the concept of a porous model. Ren et al. [22] applied a smooth particle hydrodynamics method to simulate the nonlinear interaction between the waves and moored floating breakwater. Sannasiraj et al. [20], Rahman et al. [21] and Ren et al. [22] also carried out experimental measurements to validate their theoretical results. One of the few works presented in the literature studying the horizontal vibrations of the moored elastic structures is accomplished by Chen et al. [23]. They assessed the overall behaviour of a flexible marine structure in waves and established the occurrence of rigid and flexible resonances for different frequencies of the incident wave. Jin et al. [24] created the model with the discrete-modulus-based (DMB) method in which the deformable floating structure is treated as a series of rigid modules, moving independently in six-degrees-of freedom, connected by a beam of equivalent stiffness of the actual structure. In that approach, mooring lines consist of a certain number of high-order elements in the finite-element formulation, modelled by a rod theory. It is worth mentioning that the generalized mode method used for hydroelastic analysis of the floating structures in three dimensions was based on the same principle, see [25–28].

Some authors used a more rigorous approach, considering the entire dynamic behaviour of the mooring lines. In a three-dimensional model by Loukogeorgaki and Angelides [29], the motion of the mooring system in six degrees of freedom was described by a 6×6 stiffness matrix, based on the motions of the moored body. According to that model, the displacement of the moored body, caused by the second-order drift forces, induces modifications to the initial configuration of the mooring lines and consequently leads

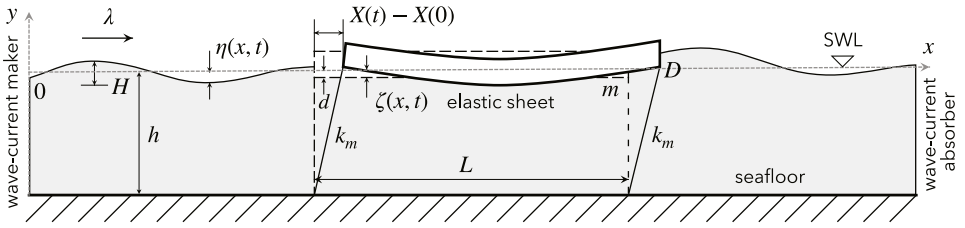

Fig. 1. Schematic of wave–current interaction with a deformable sheet connected to the seafloor by mooring lines.

to changes of their tensions. In a fully-coupled method used by Kim et al. [30], the solution is obtained by coupling the equations of the floating body and the mooring system. All of these demonstrate intensifying efforts in describing the performance of a moored floating structure in waves and the raising interest in the subject.

The principal contribution of the present paper is the model which overcomes the limitations of the previous approaches confined to the case of a ***moored fixed sheet*** by considering a ***moored free sheet*** which can oscillate in any direction around its equilibrium position due to the hydrodynamic loads of the wave–current field and the restoring force of the mooring lines. The presence of current and the ability to analyse the interplay between the wave and current effects brings this model closer to practical applications. The existing numerical models are focused on the wave–current interaction with restrained bodies or bodies with constant forward speed [31], and very few results are reported on the case of freely oscillating structures [32]. In addition, the two-dimensional model presented here is based on nonlinear equations and describes the flow-induced behaviour of a deformable structure, as opposed to linear models and models of rigid plates. In our two-dimensional study, the mooring lines are idealized as two springs connected to the sheet edges, acting in both horizontal and vertical directions as provided by a certain predetermined principle. We will neglect the catenary effect due to the weight of the mooring lines and consider the mooring of the tension type, when the mooring stiffness is constant. The focus of the paper is on understanding of the flow-induced loads, motions and deformations, and effect of the structure on the ambient flow field in the presence of mooring.

The remaining of the paper is organized as follows. In Section 2, the theoretical model associated with the interaction of nonlinear ocean waves and current with a floating deformable structure, moored to the seafloor by springs, is formulated in shallow water depth. We make a distinction between two modes of the sheet movements, namely: vertical elastic deformations and horizontal motions as a rigid body, which are discussed separately in Sections 3 and 4, respectively. The vertical deformations of the floating, elastic structures, to which extensive research data are available, are presented here mainly for comparison purposes. The investigation of the sheet surge motion on the horizontal plane is the principal focus of this paper. The presence of mooring restricts the free drift of the floating structure, but also impacts its surge and generates some interesting effects, that are discussed in Section 4. In Section 5, the wave reflection and transmission from the floating structure are presented to investigate the influence of mooring lines on the performance of the structure in scattering the ambient flow field. The key conclusions and contributions are summarized in the last section of the paper.

2. Mathematical formulation

The theoretical model under study consists of an elastic sheet floating on the surface of an inviscid, incompressible fluid and connected to the seafloor by mooring lines (Fig. 1). The sheet has length L, thickness δ, mass per unit width m, draft d and flexural rigidity D. The mooring lines have the form of an extensible spring of stiffness k_m. A two-dimensional Cartesian coordinate system is introduced whose origin is located on the undisturbed free surface, x-axis is pointed to the right and y-axis is directed upwards. The fluid density ρ, depth h, and acceleration due to gravity g are used as dimensionally independent set to nondimensionalize all variables, e.g.,

$$\tilde{x} = \frac{x}{h}, \quad \tilde{\eta} = \frac{\eta}{h}, \quad \tilde{\zeta} = \frac{\zeta}{h}, \quad \tilde{t} = t\sqrt{\frac{g}{h}}, \quad \tilde{u} = \frac{u}{\sqrt{gh}}, \quad \tilde{m} = \frac{m}{\rho h}, \quad \tilde{D} = \frac{D}{\rho g h^4}, \quad \tilde{k}_m = \frac{k_m}{\rho g h^2}, \tag{1}$$

where $\eta(x,t)$ is the free surface elevation measured from the still-water level (SWL), $\zeta(x,t)$ is the sheet deflection measured from its stationary position, and $u(x,t)$ is the horizontal fluid velocity. For consistency and simplicity, all equations, input parameters, and resulting figures will be given in dimensionless form with the tildes dropped. In this study, attention is confined to wave–current interaction with a single sheet. In general, however, there may be arbitrary number of sheets, see [14,33] for discussion on wave interaction with multiple floating sheets that use an approach similar to this study.

A numerical wave–current tank is equipped with a wave–current maker, which can create nonlinear cnoidal waves of height H and length λ (or period T) and uniform current of speed U_c, and a wave–current absorber, which minimizes the reflection of the flow back into the domain. The sheet can bend elastically and drift freely with respect to the stationary seafloor as a result of the wave and current action within the limits of the mooring restoring forces.

The problem is solved with the following list of assumptions: (i) the elastic sheet and the fluid are in touch at all points including the sheet edges, meaning that no air gap can be formed under the sheet; (ii) the friction at the contact surface between the sheet

and the inviscid fluid is assumed negligible, meaning that the flow-induced force on the sheet is due to hydrodynamic pressure only; (iii) the fluid is not allowed to flow on the upper surface of the sheet, meaning there is no overtopping; (iv) the horizontal length of the sheet remains constant, meaning that any possible deformation occurring in the sheet is limited to the vertical bending; (v) the mooring lines are thin and create no disturbance to the flow.

The problem of the free drift of a single and multiple elastic sheets under the combined action of waves and current has been investigated in our recent works [13,14]. In this paper, we introduce the necessary changes to the equations governing the flow and the motion of the sheet to account for the forces from the mooring lines. Following the same basic principles, we assume that the flow consists of two types of regions, namely RI under the free surface, and RII under the sheet. The flow in each region is governed by its own set of equations. The solution is obtained by solving the equations simultaneously in the entire flow domain and connecting the regions using the appropriate boundary and matching conditions. This decomposition method has been successfully applied by Hayatdavoodi and Ertekin [34,35] to study solitary and cnoidal waves interacting with a submerged plate.

2.1. The Green–Naghdi equations

The equations of motion of the inviscid, incompressible fluid bounded above partly by the free surface and partly by a floating sheet, are provided here by the Level I Green–Naghdi theory (GN hereafter) [36,37]. In this theory, irrotationality of the flow is not required in general, although this assumption can be made in a special version of the equations known as the Irrotational Green–Naghdi Equations (IGN), see [38,39]. For some applications to nonlinear wave diffraction and refraction, including comparisons of IGN of variable levels and the Level I GN equations, see [40–42].

The domain of the wave–current interaction with the elastic plate can be conventionally decomposed into two types of Regions: RI - formed by a flat and stationary seafloor and the free surface, on top of which the pressure is atmospheric; RII - formed by a flat and stationary seafloor and the floating elastic surface [13,14,33]. The leading and trailing edges of the sheet are at $x_L(t)$ and $x_T(t)$, respectively, the boundaries between RI and RII Regions. The nondimensional depth of the fluid under the sheet at rest is $h_1 = 1-d$. Because of the differences in the fluid layer thicknesses and boundary conditions on the upper surfaces, the equations of fluid motion over a flat and stationary seafloor in both regions are formulated differently and consist of conservation of mass [43,44]:

$$\eta_{,t} + (1+\eta)u_{,x} + u\eta_{,x} = 0, \quad \text{in RI}, \quad x < x_L \ \& \ x > x_T, \tag{2}$$

$$\zeta_{,t} + (h_1+\zeta)u_{,x} + u\zeta_{,x} = 0, \quad \text{in RII}, \quad x_L \le x \le x_T, \tag{3}$$

and conservation of linear momentum

$$3\dot{u} + 3\eta_{,x} + 2\eta_{,x}\ddot{\eta} + (1+\eta)\ddot{\eta}_{,x} = 0, \quad \text{in RI}, \quad x < x_L \ \& \ x > x_T, \tag{4}$$

$$3\dot{u} + 3\zeta_{,x} + 3\hat{p}_{,x} + 2\zeta_{,x}\ddot{\zeta} + (h_1+\zeta)\ddot{\zeta}_{,x} = 0, \quad \text{in RII}, \quad x_L \le x \le x_T, \tag{5}$$

which are solved for the unknown free surface elevation $\eta(x,t)$, sheet deflection $\zeta(x,t)$, and horizontal fluid velocity $u(x,t)$. Subscripts after comma denote partial derivatives with respect to the given variable and upper dot specifies the total time (or material) derivative.

In Eq. (5), the pressure $\hat{p}$ at the fluid-sheet contact surface can be expressed through the sheet deflection $\zeta(x,t)$ by the thin plate theory as [45]:

$$\hat{p} = m\zeta_{,tt} + D\zeta_{,xxxx} + m, \tag{6}$$

where the flexural rigidity of the sheet is defined through its thickness δ, Young's modulus E and Poisson's ratio ν by $D = E\delta^3/12(1-\nu^2)$. Once the unknown free surface elevation $\eta(x,t)$ and sheet deflection $\zeta(x,t)$ are determined, the vertical fluid velocity $v(x,y,t)$ and hydrodynamic pressure $p(x,y,t)$ can be determined explicitly [7,33]:

$$v(x,y,t) = \dot{\eta}(1+y)/(1+\eta), \quad \text{in RI}, \quad x < x_L \ \& \ x > x_T, \tag{7}$$

$$v(x,y,t) = \dot{\zeta}(1+y)/(h_1+\zeta), \quad \text{in RII}, \quad x_L \le x \le x_T, \tag{8}$$

$$p(x,y,t) = \frac{1}{2}(1+\eta)(\ddot{\eta}+2) - (1+y) - \frac{1}{2}(1+y)^2\ddot{\eta}/(1+\eta), \text{ in RI}, x < x_L \ \& \ x > x_T, \tag{9}$$

$$p(x,y,t) = \frac{1}{2}(h_1+\zeta)(\ddot{\zeta}+2) + \hat{p} - (1+y) - \frac{1}{2}(1+y)^2\ddot{\zeta}/(h_1+\zeta), \text{ in RII}, x_L \le x \le x_T. \tag{10}$$

Thereby, in the Level I GN theory, the vertical fluid velocity is linearly distributed along the water column and horizontal fluid velocity is uniform along the water depth. In the high-level GN theory, the vertical velocity distribution is described by higher-order polynomials (or, alternatively, exponential functions). While Level I GN equation are suitable for propagation of long waves in shallow water, high-level GN equations are generally applicable to nonlinear, unsteady flows in arbitrary water depths, see [46–48] for more information. For applications of the GN equations to internal waves, see e.g. [49].

2.2. Boundary and matching conditions

By virtue of the GN equations, the exact nonlinear kinematic and dynamic boundary conditions at the upper surfaces of Regions RI and RII, as well as the impermeability condition on the bottom, are already satisfied exactly by the system of Eqs. (2)–(10). In order to construct the solution, valid in the entire fluid domain, the solutions obtained in each region should be connected through

appropriate jump and matching conditions. Across the discontinuity curves dividing the regions, we enforce the continuity of mass flux

$$\eta(u-U)|_{x_L-\varepsilon} = \zeta(u-U)|_{x_L+\varepsilon}, \tag{11a}$$

$$\zeta(u-U)|_{x_T-\varepsilon} = \eta(u-U)|_{x_T+\varepsilon}, \tag{11b}$$

where U is the horizontal velocity of the sheet, and continuity of the bottom pressure

$$\frac{1+\eta}{2}(\ddot{\eta}+2)|_{x_L-\varepsilon} = \left[\frac{h_1+\zeta}{2}(\ddot{\zeta}+2)+\hat{p}\right]_{x_L+\varepsilon}, \tag{12a}$$

$$\left[\frac{h_1+\zeta}{2}(\ddot{\zeta}+2)+\hat{p}\right]_{x_T-\varepsilon} = \frac{1+\eta}{2}(\ddot{\eta}+2)|_{x_T+\varepsilon}. \tag{12b}$$

Provided that $\varepsilon \ll 1$ is an infinitesimal quantity, $x_L \pm \varepsilon$ and $x_T \pm \varepsilon$ denote the single-sided limiting values of the coordinates of the leading edge x_L and trailing edge x_T, respectively. A derivation of jump conditions for wave interaction with a submerged plate can be found in [50].

In this study, there are two mooring lines attached to the bottom edges of the sheet. The presence of mooring lines connecting the sheet to the seafloor, introduce a correction to the boundary conditions at the free-free ends of the floating sheet. The bending moment remains zero at the sheet ends:

$$D\zeta_{,xx}\Big|_{x_L} = 0, \tag{13a}$$

$$D\zeta_{,xx}\Big|_{x_T} = 0. \tag{13b}$$

In addition, the shear forces or transverse component of the tension must be balanced by the restoring forces of the mooring, i.e.

$$D\zeta_{,xxx}\Big|_{x_L} = -k_m\zeta(x_L,t), \tag{14a}$$

$$D\zeta_{,xxx}\Big|_{x_T} = -k_m\zeta(x_T,t). \tag{14b}$$

For simplicity, we assume that the stiffnesses of the two mooring lines attached to both ends of the sheet are equal, although this is not required in general. Note that in the absence of mooring ($k_m = 0$), the shear forces would vanish. Boundary conditions (13) and (14) are conventionally used in the models of deformable floating structures with vertical mooring lines, see [15–19,51].

Additional boundary conditions, specifying that the fluid remains in contact with the sheet at the edges, should be enforced. The derivation follows from taking successively the second- and third-order spatial derivatives of mass Eq. (3) and substituting the bending moments and shear forces evaluated from conditions (13) and (14). The resulting equations take the form:

$$-k_m\zeta u + 3D\zeta_{,x}u_{,xx} + D(h_1+\zeta)u_{,xxx} = 0, \quad (x = x_L, \quad x = x_T), \tag{15}$$

$$-k_m\zeta_{,t} + D\zeta_{,xxxx}u - 4k_m\zeta u_{,x} + 4D\zeta_{,x}u_{,xxx} + D(h_1+\zeta)u_{,xxxx} = 0, \quad (x = x_L, \quad x = x_T). \tag{16}$$

On the left side of the domain, a numerical wave–current maker generates periodic nonlinear (cnoidal) waves with an optional uniform current. The periodic solution of Eqs. (2) and (4) can be written in the moving coordinate system as follows [35,52,53]:

$$\eta(x-ct) = \eta_2 + H\mathbf{Cn}^2, \tag{17a}$$

$$u(x-ct) = \frac{c\cdot\eta(x-ct)}{1+\eta(x-ct)}, \tag{17b}$$

where $\mathbf{Cn}$ is the Jacobian elliptic function and c is the phase speed, obtain by solving the following relations iteratively:

$$c = \sqrt{(1+\eta_1)(1+\eta_2)(1+\eta_3)}, \tag{18a}$$

$$\eta_1 = -\frac{H}{k^2}\frac{E(k)}{K(k)}, \tag{18b}$$

$$\eta_2 = \frac{H}{k^2}\left(1-k^2-\frac{E(k)}{K(k)}\right), \tag{18c}$$

$$\eta_3 = \eta_2 + H, \tag{18d}$$

$$k^2 = \frac{H}{\eta_3-\eta_1}. \tag{18e}$$

Here, $K(k)$ and $E(k)$ are the complete elliptic integrals of the first and second kind, respectively. The wavelength λ can be calculated using the GN dispersive relation

$$\lambda = ckK(k)\sqrt{\frac{16}{3H}}. \tag{19}$$

When the uniform current is present, the wave–current maker maintains the corresponding inflow in the flow domain. Hence, the fluid velocity at the wavemaker is prescribed as

$$u_c(t) = u(x-ct) + U_c, \tag{20}$$

where U_c is the current velocity. The current absorber on the opposite end of the domain ensures conservation of mass in the tank by letting the fluid out of the domain with the same rate as it enters the domain. The current is favourable or adverse, when at initial time the fluid moves with uniform speed in the positive ($U_c > 0$) or negative direction ($U_c < 0$), respectively. The initial conditions are formulated as follows:

$$\eta(x,0) = 0, \tag{21a}$$

$$u(x,0) = U_c. \tag{21b}$$

In the absence of current ($U_c = 0$), the fluid is initially at rest.

On the right side of the domain, the open-boundary Orlanski's condition is prescribed to reduce reflections back into the wave tank:

$$\eta_{,t} \pm c\eta_{,x} = 0, \tag{22a}$$

$$u_{,t} \pm cu_{,x} = 0. \tag{22b}$$

2.3. Horizontal forces

The model, where the loosely moored sheet can be displaced from its initial position by combined action of waves and current, should include the equation prescribing the translational motion of the floating body. In Newton's second law, the total external force acting on the body consolidates those of the wave, current and mooring lines. The discussion of the horizontal forces on the freely floating elastic sheet without mooring has been presented in our recent work, see [13], in which we showed that the hydrodynamic force acting on the floating sheet can be calculated directly through the pressure integral over the wetted area as:

$$F_h(t) = -\int_{x_L}^{x_T} \hat{p}(x,t)\zeta_{,x}dx + (\hat{p}(x_L,t) - \hat{p}(x_T,t))\frac{d}{2}. \tag{23}$$

Fluid pressure distribution $\hat{p}(x,t)$ over the sheet's lower surface is determined from Eq. (6), based on the calculated sheet deformation $\zeta(x,t)$. In the Level I GN theory, the hydrodynamic pressure distribution along the vertical walls of the sheet down to the edges is nearly linear, see [54,55], and hence results in the last term of formula (23). Further discussion about fluid-induced loads on horizontal plates calculated by the GN equations can be found in e.g. [56,57].

In this paper, we consider the floating sheet connected to the seafloor by mooring lines, which contribute to the total horizontal force determining the translatory motion of the sheet. In the linear spring model utilized here, similar to the boundary conditions (14), the force from the spring stretched or compressed to a certain length is given by:

$$F_m(t) = -k_m(X(t) - X(0)). \tag{24}$$

Here $X(t)$ is the variable horizontal coordinate of the center of mass of the sheet. Note that in the vertical direction, the action of mooring lines is implemented through the boundary conditions (14). To reduce the number of parameters, the stiffness coefficients of the mooring lines in both horizontal and vertical directions are chosen to be equal in this study, although this is not required in general. Therefore, the translational motion of the moored sheet is obtained by solving the differential equation:

$$mL\frac{d^2X(t)}{dt^2} = F_h(t) + 2F_m(t), \tag{25}$$

where the mooring force is doubled due to the action of identical mooring lines at both sides of the sheet. In a more complex approach, the total solution can be obtained by coupling the equations of the floating body and the mooring system, see e.g. [30].

Thus, the complete set of equations formulating the coupled motion of the fluid and freely floating elastic sheets moored to the seafloor is closed. The equations for the fluid flow and vertical elastic deformations of the floating sheet (2)–(10), complemented by boundary conditions (11)–(16), (20) and (22), initial conditions (21), are solved simultaneously in the entire flow domain. The numerical solution is found with the use of a finite-difference technique and the modified Euler's time-stepping method. At each time step, the location of the sheet is determined based on the solution of Eq. (25) and the horizontal coordinates of the sheet edges are updated. Details about the numerical technique used to solve the system of equations can be found in [13,14].

3. Vertical response of the moored sheet

The moored deformable sheet on the surface responds to the action of the incident wave and current by elastic deformation, causing the varying tension in the mooring lines. Depending on the mooring stiffness, the maximum deformations and bending moment along the floating body may differ considerably. In terms of the vertical motions, the difference between the ***moored fixed sheet*** and ***moored free sheet*** is insignificant, except for the point of resonance in which the ***moored free sheet*** exhibits violent movements in both horizontal and vertical directions. Therefore, in this section, we investigate the effect of mooring lines on the vertical response of the floating sheet by considering ***moored fixed sheets***. ***Moored free sheets*** will be considered in the next section, where the effect of mooring on horizontal motion of the sheet and subsequent resonance phenomenon will be investigated.

To assess the accuracy of the proposed numerical model, we compare the vertical displacements and bending moments of different configurations of the sheets and mooring lines predicted by our approach with those in different numerical studies. Below we have summarized the data available in the literature on the floating elastic structures connected to the seafloor by vertical mooring lines.

Table 1
Parameters of the elastic sheets and wave conditions without current, used in the present comparative study.

Case	Wavelength λ	Sheet length L	Sheet mass m	Sheet rigidity D	Mooring stiffness k_m
Case 1	18	40	0.033	13.27	0.4, 4 (leading edge only)
Case 2	12	15	0.025	5	1.325
Case 3	4.42	5.13	0.008	0.07	0.1, 0.3

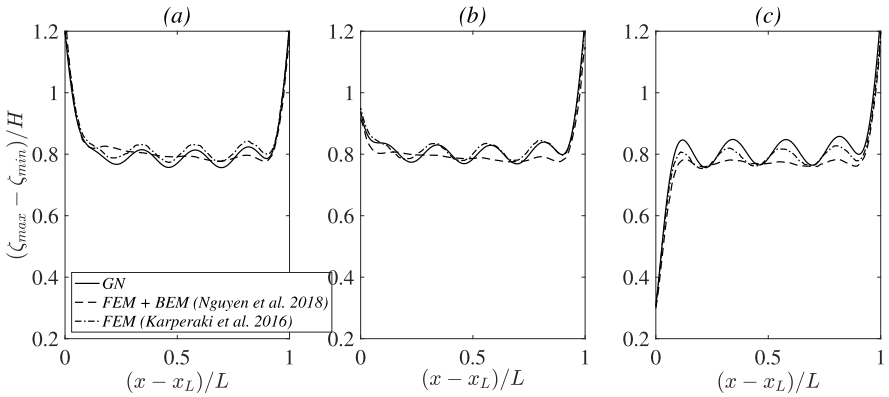

Fig. 2. Deflection amplitude of the sheet in Case 1 without current: (a) $k_m = 0$; (b) $k_m = 0.4$; (c) $k_m = 4$.

Both rectangular pontoon-type floating structures in three dimensions and thin elastic strips in two dimensions have been taken into consideration. Table 1 lists the dimensionless parameters of different wave-sheet-mooring configurations considered for the comparisons.

Fig. 2 shows the variations of the normalized deflection amplitude along the sheet length as compared with those obtained by Nguyen et al. [18] with the hybrid finite element-boundary element method and by Karperaki et al. [17] with the higher-order finite-element scheme. The notations ζ_{max} and ζ_{min} specify the maximum and minimum deformations of the sheet, respectively. In the linear case, the quantity $(\zeta_{max}-\zeta_{min})/H$ tends to the normalized deflection amplitude plotted by Nguyen et al. [18] and Karperaki et al. [17]. In this particular case, only the leading edge of the sheet is attached to the seafloor by a spring, while the trailing edge remains unrestrained. Three different values of the mooring stiffness k_m are considered with $k_m = 0$ implying the absence of mooring.

As Fig. 2 demonstrates, the present results are in good agreement with those obtained by other methods. With an increase in the mooring line stiffness, the deflection of the sheet in the vicinity of the connected edge becomes smaller, while the deflection of the rest of the sheet remains almost invariant. This reveals that mooring is less effective in reduction of the wave-induced elastic response of the sheet when it is applied to only one edge of the sheet.

In Figs. 3 and 4, the results of the GN model are shown against the solutions of Nguyen et al. [18] and Jin et al. [24], respectively. Two cases of mooring connections at both sheet edges (Figs. 3b, 3d, 4b, 4c) and with no mooring (Figs. 3a, 3c, 4a) are considered. In Figs. 3c and 3d the maximum bending moment $M_{max} = D|\zeta_{,xx}|_{max}$ scaled by the product $dHL/2$ is presented. The agreement between the results is good in the absence of mooring and satisfactory when the mooring is present. According to Fig. 3, in the vicinity of the sheet edges, the action of mooring lines results in reduced deflection amplitude and increased bending moments. In the middle of the sheet, the presence of mooring lines do not make any significant difference both in deformations and bending moments.

The presented comparisons demonstrate clearly that the GN model accounts accurately for the presence of mooring lines in compliance with the existing research results.

Fig. 5 plots the height of the sheet vertical deflection as a continuous function of the stiffness parameter at two wave gauges located at the sheet leading edge and at its center. As it might be expected, with increase of the mooring stiffness, the motion of the moored edge of the sheet becomes smaller. But reduction of the structural response does not extend to the main part of the sheet and the sheet deflection amplitude remains almost as large in the midpoint, regardless of the mooring stiffness. Hence, a mooring line is only effective in mitigation of the elastic sheet deflections in the vicinity of the connection point. Likewise, Nguyen et al. [18] established that the effectiveness of mooring lines in reducing the maximum deflection and bending moment is only significant for small and intermediate wavelengths and decreases considerably from a certain value of wavelength. The same point can be observed in Fig. 5, where three wavelengths are displayed. The reduction of the sheet vertical deflections is significant at the leading edge only and becomes weaker with an increase in the wavelength. At the center of the sheet, the mitigation of sheet vertical response is less than 10% for short waves, and almost negligible for longer waves even for large mooring stiffnesses.

Fig. 6 illustrates the effect of mooring on bending moments of the sheet for two typical wavelengths. The bending moments remain zero at the edges of the sheet in accordance with the boundary conditions (13), regardless of the value of the mooring

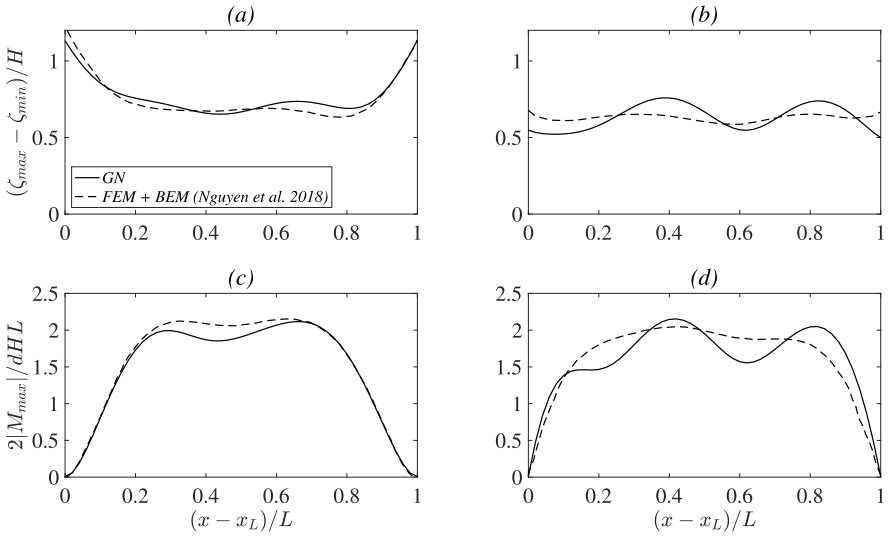

Fig. 3. Deflection amplitude and bending moments of the sheet in Case 2 without current: (a,c) $k_m = 0$; (b,d) $k_m = 1.325$.

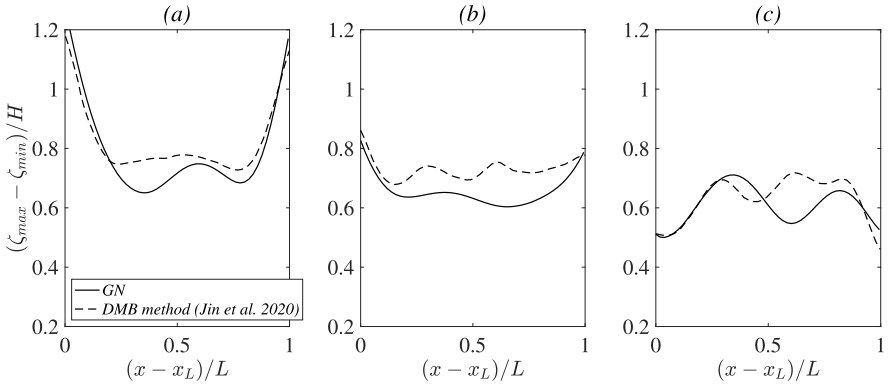

Fig. 4. Deflection amplitude of the sheet in Case 3 without current: (a) $k_m = 0$; (b) $k_m = 0.1$; (c) $k_m = 0.3$.

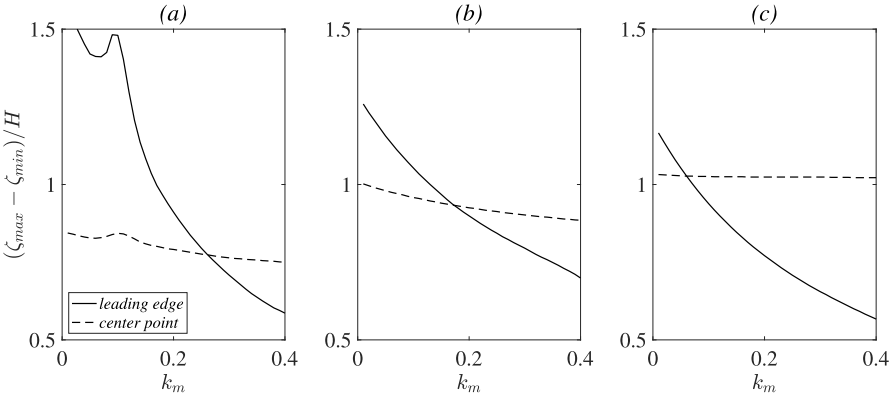

Fig. 5. Deflection amplitude of the moored fixed sheet ($L = 5$, $m = 0.05$, $D = 0.1$) at different points under the action of a cnoidal wave ($H = 0.1$) without current: (a) $\lambda/L = 1$; (b) $\lambda/L = 1.5$; (c) $\lambda/L = 2$.

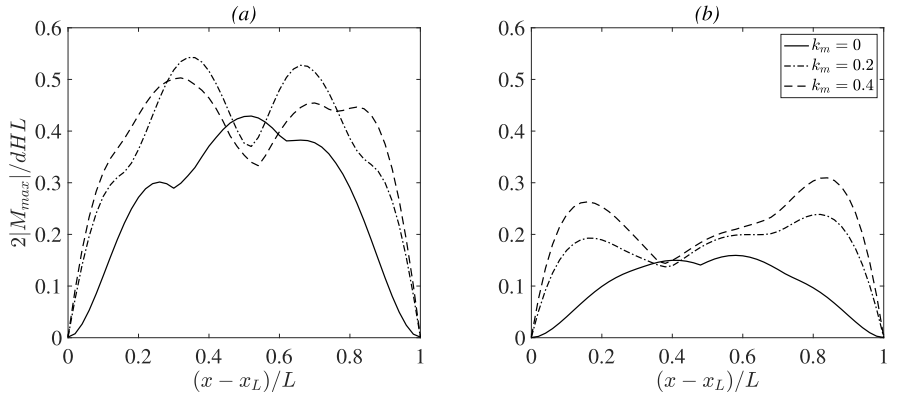

Fig. 6. Bending moments of the moored fixed sheet ($L = 5$, $m = 0.05$, $D = 0.1$) under the action of a cnoidal wave ($H = 0.1$) without current: (a) $\lambda/L = 1$; (b) $\lambda/L = 2$.

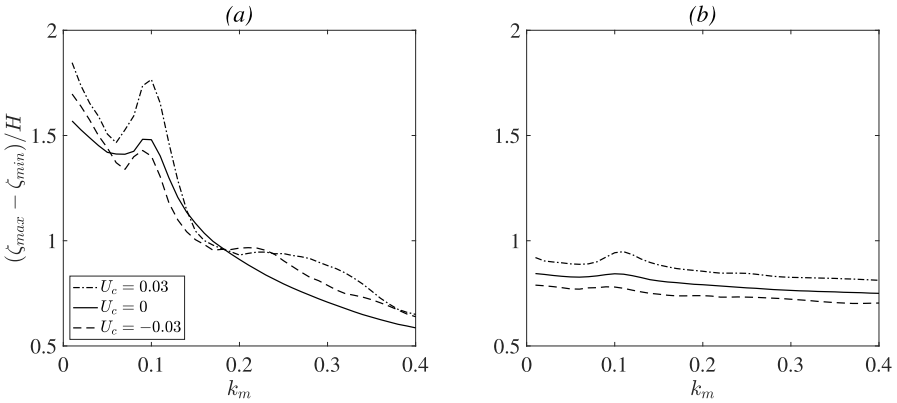

Fig. 7. Deflection amplitude of the moored fixed sheet ($L = 5$, $m = 0.05$, $D = 0.1$) under the action of a cnoidal wave ($H = 0.1$, $\lambda/L = 1$) with and without current: (a) at the leading edge; (b) at the center.

stiffness. As mooring lines become more stiff, the gradient of the bending moment increases around the edges of the sheet, while the deviations of its absolute value is comparatively small in the middle part of the sheet.

In Fig. 7, we investigate the role of the current in mitigating the hydroelastic response of the sheet by the mooring lines attached to its ends. When mooring lines are either very flexible ($k_m < 0.05$) or very stiff ($k_m > 0.2$), the sheet responds to the presence of current by increased oscillations at the edges, regardless of the current direction. For certain value of the mooring stiffness ($k_m \approx 0.2$) the current has little effect on sheet deformations. The sheet deflections at the center increase for favourable current and reduce for adverse current. The same holds true at the edges for intermediate mooring stiffness.

4. Horizontal response of the moored sheet

The freely floating sheet without mooring lines drifts as a result of the horizontal higher-order hydrodynamic forces. The detailed study on the drift response of ***unmoored free sheet*** to waves and current, including the net drift speeds and surge oscillation heights, was presented in our recent work [13]. The mooring lines prevent the drift of the floating sheet and limit its horizontal displacement to periodic oscillations around the equilibrium position. In this section, we investigate the horizontal response of the ***moored free sheet*** to the combined actions of waves and current. To distinguish between different factors governing the surge motion of the sheet, we decompose the horizontal coordinate of the oscillating sheet, $X(t)$, into the spectral image, allowing to separate the principal frequencies and corresponding amplitudes. Following the Fourier series, any continuous function $X(t)$ can be represented in the form of a series of harmonic functions:

$$X(t) = \sum_{n=1}^{\infty} \left(a_n \sin(\omega_n t) + b_n \cos(\omega_n t)\right) = \sum_{n=1}^{\infty} A_n \sin(\omega_n t + \varphi_n), \tag{26}$$

with the coefficients expressed through integrals over one incoming wave period T as

$$a_n = \frac{2}{T} \int_0^T X(t) \sin(\omega_n t) dt, \tag{27a}$$

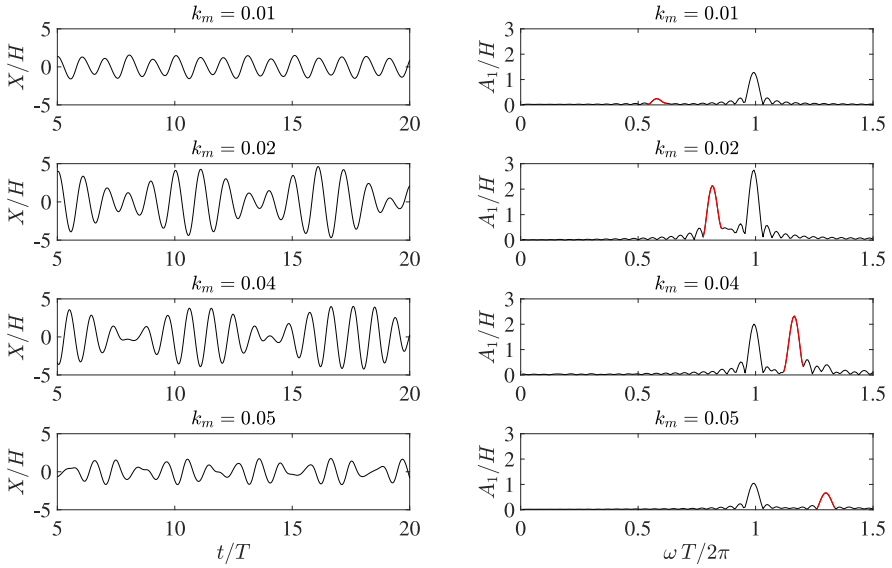

Fig. 8. Interaction of the free sheet ($L = 3$, $m = 0.05$, $D = 0.1$) moored with lines of different stiffness k_m with a cnoidal wave ($H = 0.2$, $T = 10$) without current: time series of the horizontal oscillations of the sheet (left column) and its spectra (right column).

$$b_n = \frac{2}{T}\int_0^T X(t)\cos(\omega_n t)dt, \tag{27b}$$

$$A_n = \sqrt{a_n^2 + b_n^2}. \tag{27c}$$

Here $\{\omega_n\}$ and $\{\varphi_n\}$ are the infinite series of frequencies and the corresponding phases, respectively. Given that in the GN model, solution is obtained by use of a finite-difference approach, the horizontal coordinate, $X(t)$, is defined on the discrete set of points on the limited time interval $[t_1, t_2]$, we use the Finite Fourier transform to construct the series (26)–(27). In this case, the frequencies ω_n ranges in the interval from $1/(t_2 - t_1)$ to $1/\Delta t$, where Δt is the time step. To calculate amplitudes A_n correctly, it is important that the sampling interval $[t_1, t_2]$ includes the integer number of wave periods T:

$$a_n = \frac{2}{N}\sum_{i=0}^{N-1} X_i \sin(\omega_n i\Delta t), \quad n = 1, \dots, N, \tag{28a}$$

$$b_n = \frac{2}{N}\sum_{i=0}^{N-1} X_i \cos(\omega_n i\Delta t), \quad n = 1, \dots, N. \tag{28b}$$

Here X_i is the sample value of the sheet coordinate $X(t)$ at a time $i\Delta t$ and N is the number of time steps. In this section, we will use wave period T (rather than wavelength λ) for the analysis.

In Fig. 8, time series of horizontal oscillations of the sheet $X(t)$ (left column), normalized by the incident wave height H, are accompanied by the oscillations' spectra (right column), shown as functions of frequency ω normalized by the frequency of the incident wave $2\pi/T$. The variable ω corresponds to the sheet oscillations and is represented by series $\{\omega_n\}, n = 1, N$ in formulae (26)–(28). The spectrum helps to separate the dominant frequencies by comparing the corresponding amplitudes. Observed in Fig. 8, there is a significant irregularity in the time series of sheet displacement and violation of harmonic structure of the spectra. Spectra demonstrate two peaks: the peak corresponding to the fundamental harmonics intrinsic to the incoming wave ($\omega T/2\pi = 1$) and the second peak due to the presence of mooring lines, which does not fall under any of the bounded harmonics and creates the additional oscillating component of the floating sheet. Whereas the positions of either the fundamental and bounded harmonics are fixed for the given wave conditions, the second peak changes its location with variation of the mooring stiffness k_m. As the mooring stiffness increases, the second peak appears at a greater frequency. Resonance occurs when the frequencies of fundamental and second harmonics concur. Under such conditions, the amplitude of sheet horizontal oscillations exceeds the amplitude of the wave considerably and the vibrations of the sheet become extremely violent. In this case, singularity occurs and the numerical model fails to provide the relevant solution. Similar situation can be observed in a vibrating system, when the frequency of the excitation force equals to the natural frequency of the system.

In Fig. 9, the longer sheet under the action of the longer incident wave is considered. With an increase in the mooring stiffness, as observed in Fig. 9, the peak due to the presence of mooring lines approaches successively the peaks corresponding to the frequencies of the fundamental and bounded harmonics, divided by a shorter distance in case of a long wave. Similarly, this results in the intensified surge motion of the sheet and consequent resonance. When the second harmonic interacts with the next bounded harmonic, the double frequency starts to dominate in the horizontal oscillations of the sheet. Subsequent increase in the stiffness

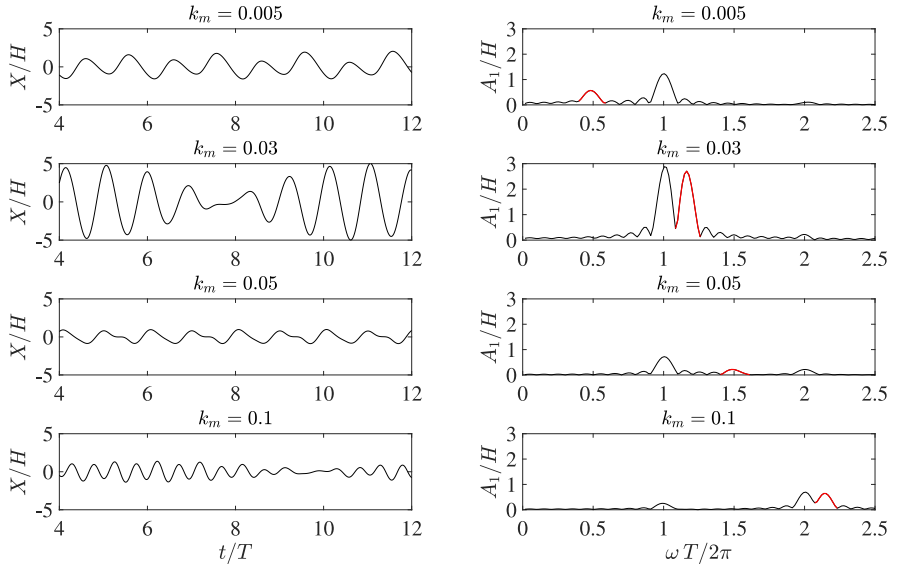

Fig. 9. Interaction of the free sheet ($L = 5$, $m = 0.05$, $D = 0.1$) moored with lines of different stiffness k_m with a cnoidal wave ($H = 0.2$, $T = 15$) without current: time series of the horizontal oscillations of the sheet (left column) and its spectra (right column).

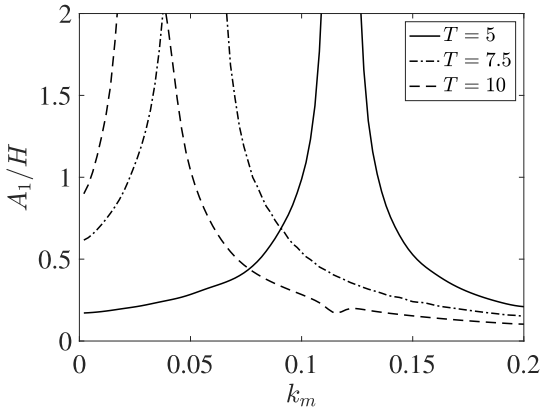

Fig. 10. Amplitude of the first harmonic of the horizontal oscillations of the moored free sheet ($L = 3$, $m = 0.05$, $D = 0.1$) under the action of a cnoidal wave ($H = 0.2$) of different period T without current.

coefficient to a larger values leads to little disturbances of the regular pattern of the sheet's horizontal oscillations and overall smaller oscillation height. Thus, any variation of the stiffness parameter, especially for longer waves, can result in a considerable change of the sheet drift behaviour. Our observations lead us to the conclusion that for any given wavelength and sheet properties, there should be the critical mooring stiffness k_c, featured by the resonant horizontal vibrations of the sheet. In subsequent analysis, we conduct the parametric study with the amplitude of horizontal oscillations of the sheet to locate the critical mooring parameter for different wave–current conditions and sheet properties.

Fig. 10 shows the variation of the first coefficient A_1 in the expansion (26), normalized by the incident wave height H, with the stiffness parameter k_m. Three incoming wave periods are considered. According to Fig. 10, in the low frequency domain, the peak surge response of the moored sheet occurs at lower stiffness parameter. As the period of the incident wave decreases, the position of the critical stiffness shifts to the large values in a nonlinear manner. When the stiffness coefficient approaches zero, the surge oscillation height increases rapidly with the wave period, similar to the case of the unrestrained floating body, see [13]. It is interesting to observe that below the critical value of the stiffness parameter, stiffer mooring lines result in the intensified horizontal vibrations. Above the critical point, the surge response tends asymptotically to zero with increase in the mooring stiffness, regardless of the incoming wave period.

Next, we investigate the various effects of the sheet physical parameters (length L, unit mass m, and rigidity D) on the location of the critical mooring stiffness k_c and the magnitude of the peak surge oscillations. Figs. 11 and 12 show the plots of the principal amplitude of surge oscillations A_1 against stiffness parameter k_m for the wave of period $T = 5$, chosen small enough to locate the

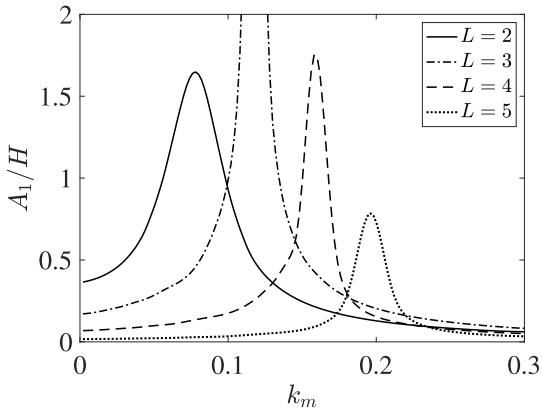

Fig. 11. Amplitude of the first harmonic of the horizontal oscillations of the moored free sheet ($m = 0.05$, $D = 0.1$) of different length L under the action of a cnoidal wave ($H = 0.2$, $T = 5$) without current.

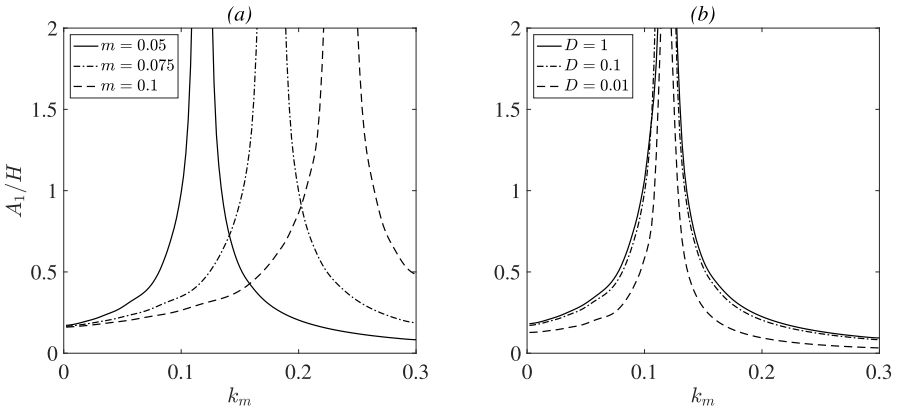

Fig. 12. Amplitude of the first harmonic of the horizontal oscillations of the moored free sheet of length $L = 3$ with: (a) different unit mass m (rigidity $D = 0.1$); (b) different rigidity D (unit mass $m = 0.05$) under the action of a cnoidal wave ($H = 0.2$, $T = 5$) without current.

sub- and overcritical regions according to Fig. 10. Fig. 11 demonstrates that for a longer sheet, remarkably larger stiffness of the mooring lines is required to achieve the critical stage. Moreover, the peak oscillations of a longer sheet is smaller compared to its shorter counterpart. In particular, the critical amplitude of the horizontal oscillations of the sheet with length $L = 5$ does not exceed the amplitude of the incoming wave. In the small mooring stiffness limit, longer sheets exhibit little horizontal movements. This can be accounted for by a comparatively small total hydrodynamic force and thereafter very small drift speed which the longer sheets exhibit when they are not moored to the seafloor and can drift freely, see [14].

Fig. 12(a) shows that horizontal vibrations of the moored sheet depend on the sheet unit mass m (draft d) in a direct and linear way. Larger mass leads to larger draft, and hence to larger fluid-body contact surface and hence stiffer springs would be required to destabilize the moored system. As seen in Fig. 12(b), there is a weak correlation between the rigidity of the sheet D and the stiffness of the mooring lines k_m in terms of the horizontal response of the sheet. The sheet of any rigidity experiences the maximum surge movements at the same critical mooring stiffness, but more flexible sheets undergo smaller horizontal vibrations under the same wave conditions. Starting from a certain value, the rigidity parameter plays little role in determining the horizontal motion of the moored sheet, which means that elastic sheets of high rigidity in our model can serve as a good approximation for the rigid sheets.

Fig. 13 shows the amplitude corresponding to the first harmonic of the horizontal surge oscillations of the moored sheet for both favourable and adverse current conditions. We have established earlier [13] that the presence of current can either stimulate or suppress the surge and drift motion of the free unmoored sheet depending on the current direction. Similarly, the moored sheet oscillates in the horizontal direction with greater amplitude in response to the waves with favourable current, and with smaller amplitude in response to the waves with the adverse current. Consequently, the resonant behaviour of the moored sheet may be smoothed down due to the adverse current of sufficient speed.

5. Wave field around the moored sheet

The important indicators describing the wave scattering by a floating object are the wave reflection and transmission. In this study, the reflection and transmission coefficients are defined to represent the wave scattering, according to the four (two) gauges

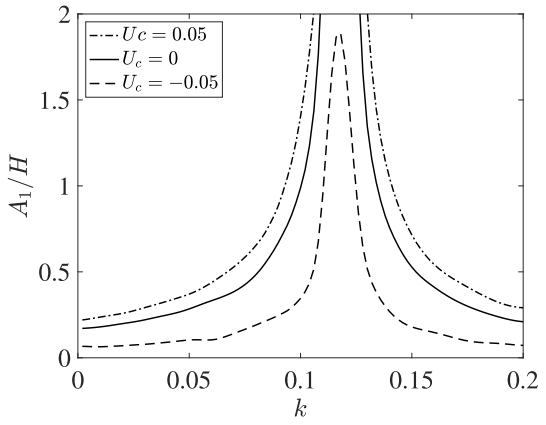

Fig. 13. Amplitude of the first harmonic of the horizontal oscillations of the moored free sheet ($L = 3$, $m = 0.05$, $D = 0.1$) under the action of a cnoidal wave ($H = 0.2$, $T = 5$) with and without current.

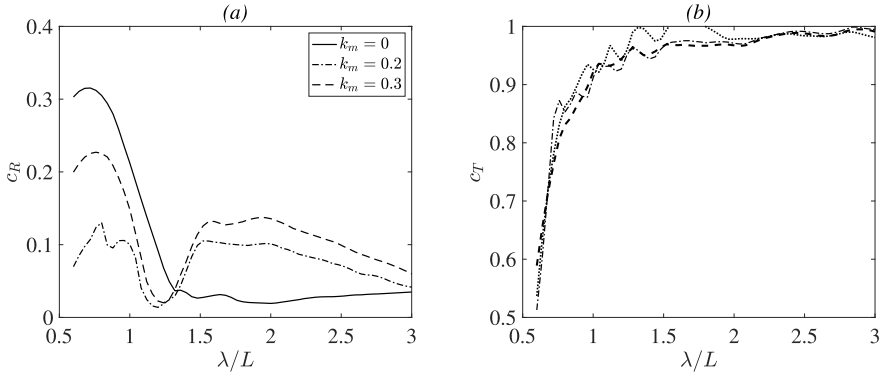

Fig. 14. (a) Reflection and (b) transmission coefficients for the moored free sheet ($L = 5$, $m = 0.05$, $D = 0.1$) with different mooring stiffness under the action of a cnoidal wave ($H = 0.1$) without current.

approach proposed by Grue [58], as $c_R = H_R/H$ and $c_T = H_T/H$, respectively, where H_R and H_T are the reflected and transmitted wave heights, calculated based on the results of the GN model at two wave gauges upwave and two wave gauges downwave the floating body. For the detailed description of the coefficients, the reader is referenced to [33,59], where this method was successfully applied to Level I GN models.

Fig. 14 shows the reflection and transmission coefficients as functions of the incoming wavelength to sheet length ratio for the moored free sheet with mooring lines of different stiffnesses. We recall from Section 4 that resonance is observed for certain mooring stiffness values, where the oscillation become unrealistically large. Therefore, we will provide the results for the range of sufficiently large mooring stiffness parameter ($k_m > 0.1$). Generally, the reflection coefficient decreases with increasing wavelength, while transmission coefficient increases proportionally due to the balance of energy of the reflected and transmitted waves. By contrast of the coefficients for the moored and unmoored sheets, displayed in Fig. 14, it can be observed that the presence of mooring has opposite effects under different wave conditions: the mooring lines slightly intensify the reflection of long waves ($\lambda/L > 1.3$), but reduce significantly the reflection of short waves ($\lambda/L < 1.3$).

Fig. 15 shows the variation of the reflection coefficient with mooring stiffness for the moored free sheet in different wave conditions without current. In the short range of mooring stiffnesses below the critical point, the reflection coefficient decreases with mooring stiffness. As it was shown in the previous section, the location of the critical point depends inversely on the incoming wavelength. In the vicinity of the critical mooring stiffness, specific for each wavelength, the proportion of the wave energy reflected by the sheet becomes unstable due to the resonance in the sheet horizontal oscillations and hence is missing in the plots. For large values of the mooring stiffness, the reflection coefficient grows almost linearly, regardless of the wave conditions.

It is evident from our previous results [13,14] that favourable current has stimulating effect on wave reflection, because the freely floating sheet drifts faster and surge wider when the current flows in the same direction as the incident wave. The adverse current has an opposite effect. Fig. 16 illustrates the trivial interplay between the factors of mooring and ambient current in terms of the reflection coefficient for one specific wavelength. As seen in Fig. 16, the reflection coefficient grows linearly with the mooring parameter as well as with the current speed. The larger the mooring stiffness, the stronger the wave reflection coefficient depends on the current speed. Hence, the desired reflection performance of the floating sheet can be achieved by adjusting the stiffness of the mooring lines in the variable wave–current conditions.

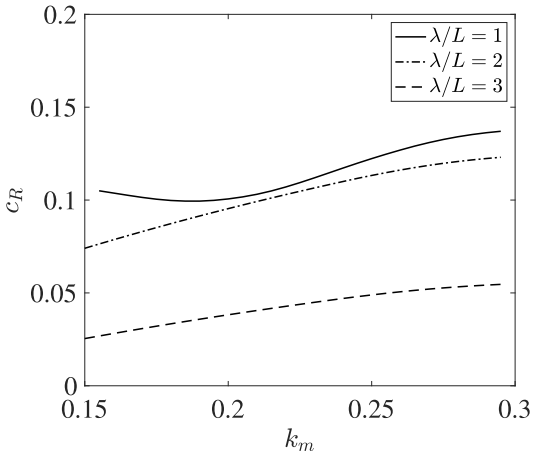

Fig. 15. Reflection c_R coefficient for the moored free sheet ($L = 5$, $m = 0.05$, $D = 0.1$) under the action of cnoidal waves ($H = 0.1$) of different wavelength without current.

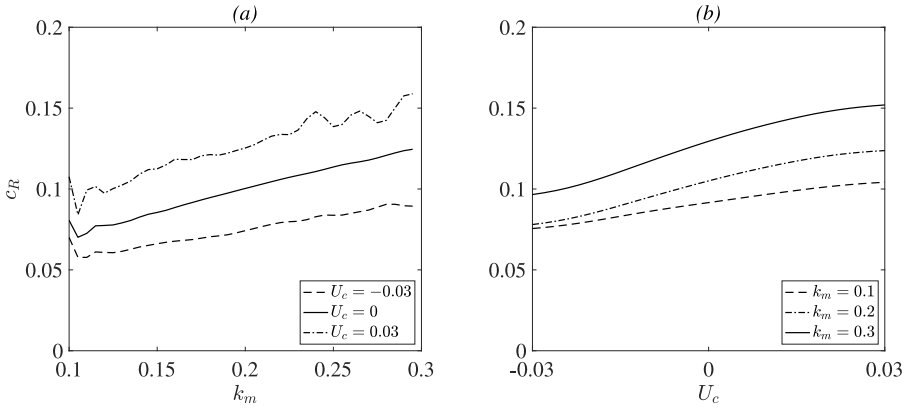

Fig. 16. Reflection coefficient for the moored free sheet ($L = 5$, $m = 0.05$, $D = 0.1$) with different mooring stiffness under the action of a cnoidal wave ($H = 0.1$, $\lambda/L = 1.5$) with and without current. $Uc = 0$ corresponds to the case of no current.

6. Conclusions

This study presents a two-dimensional model describing the nonlinear dynamics of a freely floating deformable sheet attached to the seafloor by mooring lines under the effect of combined waves and current. The floating sheet bends elastically and moves in space as a result of the wave–current action. Mooring lines act on the sheet by moderating its hydroelastic deformations and horizontal displacement. Therefore, in this paper, the motion of the moored sheet in both the horizontal and vertical directions has been investigated.

It is established that mooring lines attached to the sheet edges reduce the sheet elastic deformations in the vicinity of the sheet ends significantly, but are comparatively ineffective in mitigating the deformation along the midsections of the sheet even for large mooring stiffness. Comparisons with existing theoretical results validate this conclusion. We have discovered that the moored structure which can be offset from its initial horizontal position by the action of wave and current, can experience extreme vibrations for certain critical value of the mooring stiffness. The resonance occurs when the frequency of the excitation wave force concurs with the natural frequency of the moored sheet. Because of this, we can observe a counterintuitive increase in the magnitude of the sheet surge movements with increasing mooring stiffness below the critical value. The approximate location of the critical stiffness parameter is determined through a parametric study of the sheet properties, wave conditions and current speed. This study has shown that resonance is more likely to occur with shorter sheets in the high frequency domain. Sheet rigidity and current speed play insignificant role in determining the resonance regime of the moored sheet and mostly affect the magnitude of its vibrations.

The mooring arrangement can have significant influence on the operation and survivability of the floating solar panels and offshore structures in various environmental conditions, including waves and currents. The motion of wave-energy converters and floating wind turbines may have substantial effect on the efficiency of power capture. It is desirable to reduce the structural vibrations of the floating airports and storage facilities by installing the appropriate mooring system. The obtained results may provide the methodology to estimate the range of the optimal mooring stiffness parameter for a given floating structure based on its basic

physical properties, wave period and current speed. It is expected that results obtained in this paper for the simple model of the moored floating structure can be extrapolated to more general situations, and become beneficial at the initial stage of a structural design.

Note that while this study is confined to two dimensions, in principle, there is no restriction in applying the GN theory to three-dimensional problems. This would be achieved by considering appropriately the fluid flow in the third dimension. See e.g., [42,44,54], for three-dimensional applications of the GN theory.

Declaration of competing interest

The authors declare that they have no known competing financial interests or personal relationships that could have appeared to influence the work reported in this paper.

Data availability

The data that support the findings of this study are available within the article.

References

[1] Cazzaniga R, Cicu M, Rosa-Clot M, Rosa-Clot P, Tina G, Ventura C. Floating photovoltaic plants: Performance analysis and design solutions. Renew Sustain Energy Rev 2018;81:1730–41.
[2] Vo T, Ko H, Huh J, Park N. Overview of possibilities of solar floating photovoltaic systems in the offshore industry. Energies 2021;14(6988):1–30.
[3] Meylan M, Squire VA. The response of ice floes to ocean waves. J Geophys Res 1994;99(C1):891–900.
[4] Wu C, Watanabe E, Utsunomiya T. An eigenfunction expansion-matching method for analyzing the wave-induced responses of an elastic floating plate. Appl Ocean Res 1995;17:301–10.
[5] Korobkin AA. Unsteady hydroelasticity of floating plates. J Fluids Struct 2000;14:971–91.
[6] Riggs HR, Suzuki H, Ertekin RC, Kim JW, Iijima K. Comparison of hydroelastic computer codes based on the ISSC VLFS benchmark. Ocean Eng 2008;35(7):589–97.
[7] Xia D, Ertekin RC, Kim JW. Fluid-structure interaction between a two-dimensional mat-type VLFS and solitary waves by the Green-Naghdi theory. J Fluids Struct 2008;24(4):527–40.
[8] Sturova IV. Time-dependent response of a heterogeneous elastic plate floating on shallow water of variable depth. J Fluid Mech 2009;637:305–25.
[9] Ertekin RC, Xia D. Hydroelastic response of a floating runway to cnoidal waves. Phys Fluids 2014;26:027101.
[10] Marchenko AV. The floating behaviour of a small body acted upon by a surface wave. J Appl Maths Mechs 1999;63(3):471–8.
[11] Yiew LJ, Bennets LG, Meylan MH, French BJ, Thomas GA. Hydrodynamic responses of a thin floating disk to regular waves. Ocean Model 2016;97:52–64.
[12] Ren B, He M, Dong P, Wen H. Nonlinear simulations of wave-induced motions of a freely floating body using WCSPH method. Appl Ocean Res 2015;50:1–12.
[13] Kostikov VK, Hayatdavoodi M, Ertekin RC. Drift of elastic floating ice sheets by waves and current, part I: single sheet. Proc R Soc A 2021;477:20210449.
[14] Kostikov VK, Hayatdavoodi M, Ertekin RC. Drift of elastic floating ice sheets by waves and current: multiple sheets. Phys Fluids 2022;34:057113.
[15] Khabakhpasheva TI, Korobkin AA. Hydroelastic behaviour of compound floating plate in waves. J Engrg Math 2002;44:21–40.
[16] Karmakar D, Soares CG. Scattering of gravity waves by a moored finite floating elastic plate. Appl Ocean Res 2012;34:135–49.
[17] Karperaki AE, Belibassakis KA, Papathanasiou TK. Time-domain, shallow-water hydroelastic analysis of VLFS elastically connected to the seabed. Mar Struct 2016;48:33–51.
[18] Nguyen HP, Dai J, Wang CM, Ang KK, Luong VH. Reducing hydroelastic responses of pontoon-type VLFS using vertical elastic mooring lines. Mar Struct 2018;59:251–70.
[19] Mohapatra SC, Soares CG. Effect of mooring lines on the hydroelastic response of a floating flexible plate using the BIEM approach. J Mar Sci Eng 2021;9(941):1–14.
[20] Sannasiraj SA, Sundar V, Sundaravadivelu R. Mooring forces and motion responses of pontoon-type floating breakwaters. Ocean Eng 1998;25(1):27–48.
[21] Rahman MA, Mizutani N, Kawasaki K. Numerical modeling of dynamic responses and mooring forces of submerged floating breakwater. Coast Eng 2006;53:799–815.
[22] Ren B, He M, Li Y, Dong P. Application of smoothed particle hydrodynamics for modeling the wave-moored floating breakwater interaction. Appl Ocean Res 2017;67:277–90.
[23] Chen X, Wu Y, Cui W, Tang X. Nonlinear hydroelastic analysis of a moored floating body. Ocean Eng 2002;30:965–1003.
[24] Jin C, Bakti FP, Kim MH. Multi-floater-mooring coupled time-domain hydro-elastic analysis in regular and irregular waves. Appl Ocean Res 2020;101:102276.
[25] Wang D, Riggs H, Ertekin RC. Three-dimensional hydroelastic response of a very large floating structure. Int J Offshore Polar Eng 1991;1(4):307–16.
[26] Ertekin RC, Riggs HR, Che XL, Du SX. Efficient methods for hydroelastic analysis of very large floating structures. J Ship Res 1993;37(1):58–76.
[27] Wu Y, Wang D, Riggs HR, Ertekin RC. Composite singularity distribution method with application to hydroelasticity. Mar Struct 1993;6(2-3):143–63.
[28] Huang LL, Riggs HR. The hydroelastic stiffness of flexible floating structures for linear hydroelasticity. Mar Struct 2000;13(2):91–106.
[29] Loukogeorgaki E, Angelides DC. Stiffness of mooring lines and performance of floating breakwater in three dimensions. Appl Ocean Res 2005;27:187–208.
[30] Kim BW, Sung HG, Kim JH, Hong SY. Comparison of linear spring and nonlinear FEM methods in dynamic coupled analysis of floating structure and mooring system. J Fluids Struct 2013;42:205–27.
[31] Nossen J, Grue J, Palm E. Wave forces on three-dimensional floating bodies with small forward speed. J Fluid Mech 1991;227:135–60.
[32] Liu Z, Teng B, Ning DZ, Gou Y. Wave-current interactions with three-dimensional floating bodies. J Hydrodyn 2010;22(2):229–40.
[33] Kostikov VK, Hayatdavoodi M, Ertekin RC. Hydroelastic interaction of nonlinear waves with floating sheets. Theor Comput Fluid Dyn 2021;35:515–37.
[34] Hayatdavoodi M, Ertekin RC. Nonlinear wave loads on a submerged deck by the Green-Naghdi equations. J Offshore Mech Arct Eng 2015;137(1):011102.
[35] Hayatdavoodi M, Ertekin RC. Wave forces on a submerged horizontal plate – part II: Solitary and cnoidal waves. J Fluids Struct 2015;54:580–96.
[36] Green AE, Naghdi PM. A derivation of equations for wave propagation in water of variable depth. J Fluid Mech 1976;78:237–46.
[37] Green AE, Naghdi PM. Directed fluid sheets. Proc R Soc Lond A 1976;347:447–73.
[38] Kim JW, Ertekin RC. A numerical study of nonlinear wave interaction in irregular seas: Irrotational Green-Naghdi model. Mar Struct 2000;13(4-5):331–47.
[39] Kim JW, Bai KJ, Ertekin RC, Webster WC. A derivation of the Green-Naghdi equations for irrotational flows. J Engrg Math 2001;40:17–42.
[40] Ertekin RC, Hayatdavoodi M, Kim JW. On some solitary and cnoidal wave diffraction solutions of the Green-Naghdi equations. Appl Ocean Res 2014;47:125–37.

[41] Zhao BB, Zhang TY, Duan WY, Ertekin RC, Hayatdavoodi M. Application of three-dimensional IGN-2 equations to wave diffraction problems. J Ocean Eng Mar Energy 2019;5:351–63.
[42] Hayatdavoodi M, Ertekin RC. Diffraction and refraction of nonlinear waves by the Green-Naghdi equations. J Offshore Mech Arct Eng 2023;145(2):021201.
[43] Ertekin RC. Soliton generation by moving disturbances in shallow water: Theory, computation and experiment [Ph.D. thesis], University of California at Berkeley; 1984.
[44] Ertekin RC, Webster WC, Wehausen JW. Waves caused by a moving disturbance in a shallow channel of finite width. J Fluid Mech 1986;169:275–92.
[45] Timoshenko SP, Woinowsky-Krieger S. Theory of plates and shells. McGraw-Hill, NY; 1959.
[46] Shields JJ, Webster WC. On direct methods in water-wave theory. J Fluid Mech 1988;197:171–99.
[47] Zhao BB, Ertekin RC, Duan WY, Hayatdavoodi M. On the steady solitary-wave solution of the Green–Naghdi equations of different levels. Wave Motion 2014;51(8):1382–95.
[48] Zhao BB, Duan WY, Ertekin RC, Hayatdavoodi M. High-level Green–Naghdi wave models for nonlinear wave transformation in three dimensions. J Ocean Eng Mar Energy 2015;1:121–32.
[49] Zhao BB, Wang Z, Duan WY, Ertekin RC, Hayatdavoodi M, Zhang TY. Experimental and numerical studies on internal solitary waves with a free surface. J Fluid Mech 2020;899:A17.
[50] Hayatdavoodi M, Ertekin RC. Wave forces on a submerged horizontal plate – part I: Theory and modelling. J Fluids Struct 2015;54:566–79.
[51] Karmakar D, Soares CG. Oblique scattering of gravity waves by moored floating membrane with changes in bottom topography. Ocean Eng 2012;54:87–100.
[52] Sun L, Taylor RE, Taylor PH. First- and second-order analysis of resonant waves between adjacent barges. J Fluid Struct 2010;26(6):954–78.
[53] Ertekin RC, Becker JM. Nonlinear diffraction of waves by a submerged shelf in shallow water. J Offshore Mech Arct Eng 1998;120:212–20.
[54] Hayatdavoodi M, Neill DR, Ertekin RC. Diffraction of cnoidal waves by vertical cylinders in shallow water. Theor Comp Fluid Dyn 2018;32:561–91.
[55] Neill DR, Hayatdavoodi M, Ertekin RC. On solitary wave diffraction by multiple, in-line vertical cylinders. Nonlinear Dynam 2018;91(2):975–94.
[56] Hayatdavoodi M, Treichel K, Ertekin RC. Parametric study of nonlinear wave loads on submerged decks in shallow water. J Fluids Struct 2019;86:266–89.
[57] Hayatdavoodi M, Liu J, Ertekin RC. Bore impact on decks of coastal structures. J Waterw Port Coast Ocean Eng 2022;148(2):04021051.
[58] Grue J. Nonlinear water waves at a submerged obstacle or bottom topography. J Fluid Mech 1992;244:455–76.
[59] Hayatdavoodi M, Ertekin RC, Valentine BD. Solitary and cnoidal wave scattering by a submerged horizontal plate in shallow water. AIP Adv 2017;7. 065212–29.